ENERGY BALANCE IN CLUSTERS OF GALAXIES

P. M. Motl
MOTL@CASA.COLORADO.EDU
J. O. Burns
Center for Astrophysics and Space Astronomy
University of Colorado at Boulder
UCB 389, Boulder, CO, 80309
JACK.BURNS@CU.EDU

Abstract

We review different physical mechanisms that are likely to play a significant role in determining the detailed thermal state of gas in clusters of galaxies. Mergers are the dominant process impacting clusters and these collisions significantly perturb the cluster state. The continual loss of energy from the gas to radiation must also be accounted for and cooling gas can drive several positive feedback mechanisms. From simple energy arguments, AGN are likely to make a significant contribution to balance the energy lost from cluster cores. We also explore additional positive feedback mechanisms including supernovae feedback and thermal conduction. If AGN are the sole feedback mechanism, what are to be made of clusters that lack evidence for AGN activity yet have canonical cool cores? As cluster samples with high-resolution X-ray data grow larger, it is likely to be the properties of relaxed, cool-core clusters that will be the best guides to numerical simulations.

1 Physical processes impacting energy balance in clusters of galaxies

We are interested in numerical simulations of clusters of galaxies, the simulated systems being used to interpret and guide observations of clusters through their X-ray emission or the thermal Sunyaev-Zeldovich effect (SZE), for example. To complete this task, we must implement a predictive numerical model for clusters of galaxies. A significant part of this effort is to place the clusters in a realistic cosmological setting to account for the full complexity of the three-dimensional structures that form through hierarchical collapse in the cold dark matter model. However, this is only part of the story. We must also specify the input physics that govern the baryonic gas, this gas being the primary tracer for cluster observations. As we will argue, the input physics are complex and should include, at a minimum, the following mechanisms that can significantly impact energy balance. The simulations must account for energy losses from the fluid to radiation, star formation that removes rapidly cooling, collapsing gas from the hydrodynamic flow, the input of thermal energy from supernovae that accompany star formation, feedback from AGN and the transport of energy through the cluster atmosphere via electronic thermal conduction.

While all these mechanisms may be expected to play a significant role, they need not be of equal importance in all clusters. To quantify their relative importance, we consider estimates that correspond to the largest, richest clusters of galaxies as these are the systems that will be the easiest to uncover and study in any cosmological survey. For lower mass systems such as poor clusters and groups, the relative importance of the different mechanisms will change.

To place the different input physics on an equal footing, we work in units of energy and time that are normalized to the characteristic values for rich clusters. Specifically, we measure energy in units of the cluster gravitational potential energy, $|W| \sim 10^{65}$ erg, for rich clusters and time is measured in units of the dynamical time, $t_{\rm dyn} \sim 1$ Gyr. In Table 1, we list estimates of the potential importance of different physical mechanisms, relative to the energy scale of a typical rich cluster. In the following sections we give a more detailed description of how these estimates are obtained.

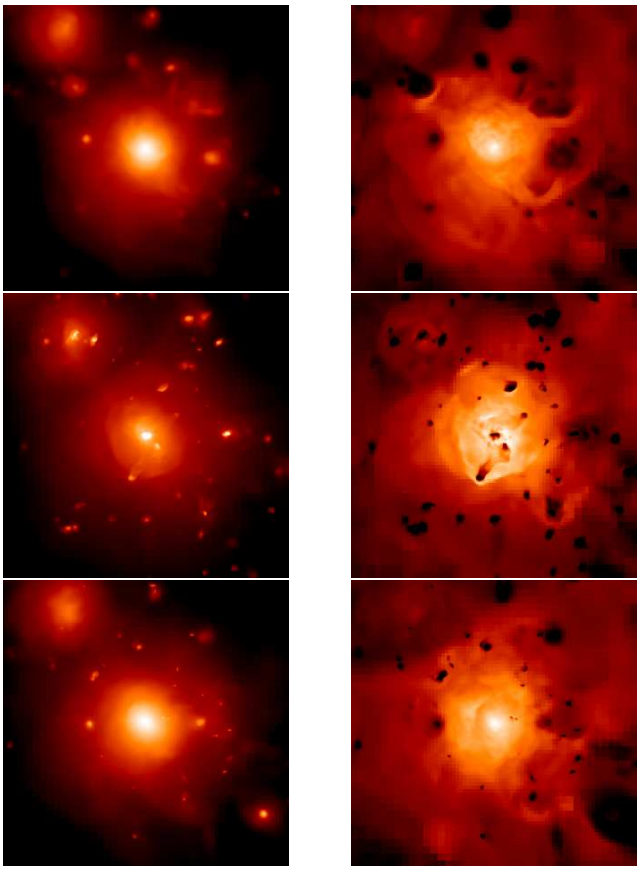

Figure 1: Images of the cluster X-ray surface brightness (left column) and the projected, emission-weighted temperature maps (right column) at the present epoch for the same cluster evolved under three physical scenarios including adiabatic physics only (top row), with radiative cooling (middle row) and with the addition of star formation and supernova feedback (bottom row). The field of view is $5h^{-1}$ Mpc on a side.

Energy Balance Scorecard

Mechanism	Contribution $[10^{65}\mathrm{erg}]$
Structure Formation	0.1
Radiative Cooling Loss	10^{-3}
Supernova Feedback	10^{-4}
Thermal Conduction	10^{-4}–10^{-3}
AGN Feedback	10^{-6}–10^{-5}

1.1 Major mergers

The process of structure formation itself is the dominant perturbation on clusters. For a typical free-fall velocity of ~ 1000 km s^{-1}, the collision of two equal mass subclusters constitutes a perturbation of up to $\sim 0.1\,|W|$. A fraction of this available energy is thermalized by the cluster medium and drives the gas out of equilibrium with the gravitational potential. Mergers also drive observable signals such as the cluster X-ray luminosity, temperature or thermal SZE to values far in excess of the expected values given the true mass of the cluster. This boosting behavior will be quantified further in Sect. 2.

1.2 Radiative cooling

Clusters of galaxies radiate in the X-ray band through thermal bremsstrahlung and line emission. For a typical cluster luminosity of $\sim 10^{45}$ erg s^{-1} over $t_{\rm dyn}$ this amounts to an energy loss of $\sim 10^{-3}\,|W|$. However, the cooling is not uniform throughout the cluster. Instead, radiative losses occur predominantly in the dense core regions. For example, compare the cluster images in the top and middle panels of Fig. 1. These images show the X-ray surface brightness and projected, emission-weighted temperature maps for the same cluster evolved in the adiabatic limit and then with the addition of radiative cooling. With cooling, substructures develop cool (dark in the temperature map), dense (bright in the X-ray images) cores of gas. These cool cores are quite resilient in cluster mergers and result in significantly stronger merger shocks during collisions (Motl et al., 2004).

1.3 Star formation and supernova feedback

In reality, gas in these cool, dense cores has a short cooling time and naturally collapses into star forming regions. We find a realistic mass fraction in star particles for simulations with a moderate amount of thermal feedback from prompt supernovae (corresponding to $\sim 4\times10^{15}$ erg g^{-1} of stars formed). This translates to an average thermal feedback of ~ 0.5 keV per particle in the clusters. If we assume that the star formation rate is uniform in time, supernova feedback can provide $\sim 10^{-4}\,|W|$ over $t_{\rm dyn}$. In reality, this overestimates the importance of supernova heating in the nearby universe as the star formation rate declines sharply in the redshift range from $0 < z < 1$.

The bottom panels of Fig. 1 illustrate the effect of star formation and supernova feedback. The dense, cool cores found in the cooling-only cluster have largely been erased and the overall cluster appearance is much closer to the adiabatic realization. While the energy input from supernova is only a small fraction of the energy lost to radiative cooling, star formation selectively removes the densest gas with the highest X-ray emis-

sivity. This effect accounts for the dramatic change in the cluster appearance between the cooling-only and star formation versions.

1.4 Thermal conduction

In addition to star formation and supernova feedback, radiative energy loss may also be compensated for by thermal conduction. Conduction will transfer energy from the hot ICM into the cluster core. Assuming that thermal conduction is only mildly suppressed relative to the Spitzer level, as indicated by recent theoretical arguments (Narayan & Medvedev, 2001) and numerical simulations (Cho et al., 2003), conduction alone may be competitive with radiative cooling.

Using the temperature gradients measured in our simulated clusters with cooling only, which give the strongest temperature gradients, we estimate the energy flux due to conduction as

$$\left(\frac{dE}{dt}\right)_{\rm conduction} = -4\pi r^2 \kappa_{\rm eff} \left(\frac{dT}{dr}\right) ergs^{-1} \quad (1)$$

with

$$\kappa_{\rm eff} = f\kappa_{\rm Spitzer} \quad (2)$$

$$= f\frac{1.84\times10^{-5}T^{\frac{5}{2}}}{\ln\Lambda} ergs^{-1}K^{-1}cm^{-1} \quad (3)$$

where $\ln\Lambda$ is the Coulomb logarithm and f is the suppression factor. Assuming f = 0.1, our cooling-only clusters would have a heat flux into the core region of $\sim 10^{44}$–10^{45} erg s^{-1} so that over $t_{\rm dyn}$ thermal conduction could deposit $\sim 10^{-4}$–10^{-3} $|W|$ into the core.

Aside from the caveat that we have estimated the energy flux in the case with the steepest temperature gradients there are several other factors that must be noted. First, magnetic fields within clusters and especially ordered fields will significantly curtail the impact of thermal conduction. Second, thermal conduction can not be strong enough to erase the small scale temperature structure seen as cold fronts and irregular temperature distributions in recent X-ray observations with *Chandra* and *XMM-Newton*. Finally, an additional constraint on $\kappa_{\rm eff}$ may arise simply from the existence of hot, massive clusters at high redshift which as Loeb (2002) pointed out, would be exceedingly difficult if conduction carried energy out of the clusters at a rate comparable to $\kappa_{\rm Spitzer}$.

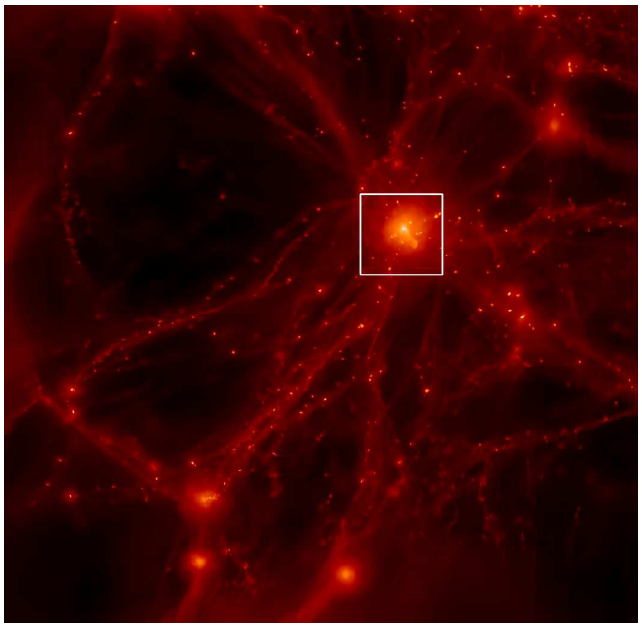

Figure 2: Projection of the gas density from the region eligible for dynamic refinement for one cluster simulation at the present epoch. The square highlights a region $5h^{-1}$ Mpc on a side while the image is $36h^{-1}$ Mpc on a side.

1.5 AGN feedback

The final component of the input physics suite that we are working to incorporate into our simulations is feedback from AGN. From published observations of X-ray bubbles in the cores of nearby clusters (McNamara et al., 2000; Fabian et al., 2000; McNamara et al., 2001; Blanton et al., 2001; Heinz et al., 2002; Johnstone et al., 2002), the energy input to inflate the bubbles is $\sim 10^{58}$–10^{59} erg. If we assume that the AGN feedback cycle time is $\sim$ 0.1 Gyr and neglect evolution in the AGN luminosity we see that over $t_{\rm dyn}$, AGN can add energy to the cluster core at a level of 10^{-6}–10^{-5} $|W|$. If the total feedback cycle time is shorter than the assumed value, the average AGN contribution will be correspondingly larger.

In recent theoretical work, Ruszkowski & Begelman (2002) have demonstrated that a combination of radiative cooling, thermal conduction and AGN heating described by a time-averaged, effervescent heating model can reproduce the observed thermal properties of the cluster gas, though their work requires strict assumptions including spherical symmetry for the cluster. More general simulations of the interaction between AGN jets and the cluster ICM have been performed and we note in particular the work of Omma et

al. (2004). We are currently incorporating the AGN jet model from their simulations into fully dynamic, cosmological cluster simulations.

To summarize, the processes of thermal conduction, supernova feedback and AGN feedback are expected to make contributions to the energy balance in clusters that are roughly comparable in magnitude. At the very least, none of the mechanisms can be discounted as insignificant in compensating the energy loss from radiative cooling. Furthermore, two of the sources of positive feedback (supernovae and AGN) are fueled at the cooling rate. In a similar manner, steep core temperature gradients created by cooling can drive a vigorous conductive heat flux from the cluster envelope into the core. We are thus faced with a complex system of coupled mechanisms that dictate the detailed thermal state of the ICM.

However, the dominant perturbation on clusters of galaxies arises from the formation of structure itself. Major mergers can impart orders of magnitude more energy than any other mechanism and can significantly perturb the cluster structure, bias observational signatures and can effectively reset the thermal state of the gas in the cluster.

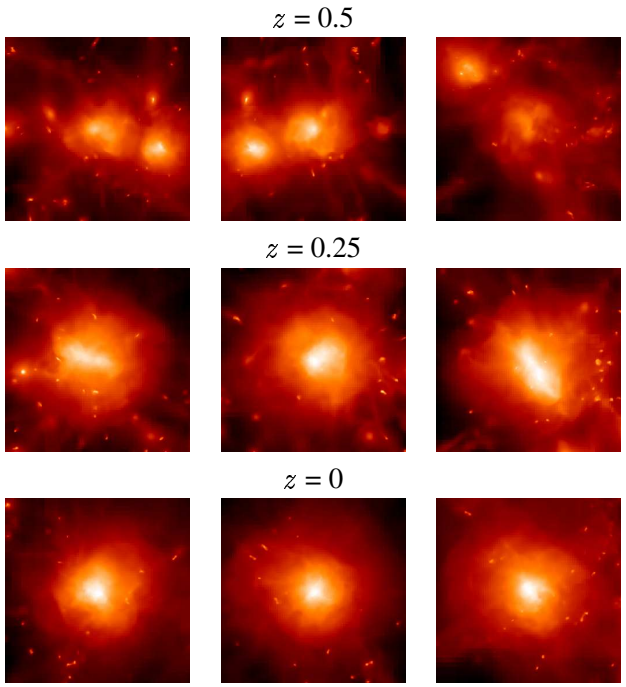

Figure 3: Projections of the gas density along three orthogonal axes for selected epochs of the simulated cluster depicted in the accompanying animations. The cluster suffers a major merger that begins shortly after $z \sim 0.5$. The images show a comoving region $5h^{-1}$ Mpc on a side.

2 Insight from cluster simulations

We now highlight some results and insights derived from our current generation of cluster simulations. We use the hybrid N-body/hydrodynamics cosmology code ENZO (http://cosmos.ucsd.edu/enzo) which implements adaptive mesh refinement (AMR) to achieve high resolution in dense regions of the simulation. Our current simulations include radiative cooling using a tabulated Raymond-Smith cooling curve appropriate for a 0.3 solar metallicity plasma and we utilize the Cen & Ostriker (1992) algorithm for star formation and supernova feedback. We employ the concordance ΛCDM cosmological model with $H_0 = h100$ km s^{-1} Mpc^{-1} = 70, Ω_m = 0.3, Ω_Λ = 0.7, Ω_b = 0.026 and σ_8 = 0.928.

Our simulations begin from a periodic sample box $256h^{-1}$ comoving Mpc on a side that has been simulated at low resolution to identify regions that form clusters. The volume is then re-simulated with the AMR infrastructure deployed about individual cluster regions. An example cluster volume is shown in Fig. 2. Two nested, static grids enclose and refine the volume of interest. Additional, dynamic refinement is employed as needed within the cluster volume and we use 7 to 11 total levels of refinement (corresponding to spatial resolutions of $\sim$ 16–$1h^{-1}$ kpc). This typically results in a few thousand grids being used to simulate the cluster and its immediate neighborhood.

Here, we focus on a simulation of our most massive cluster with up to 10 total levels of refinement ($\sim 2h^{-1}$ kpc resolution) with cooling, star formation and supernova feedback. The virial radius of the cluster is approximately r_{200} = 2.6 Mpc, corresponding to a spherical over-density of 200 relative to the critical density. Within r_{200}, this particular cluster has M_{tot} = 2.1×10^{15} $M_\odot$, M_{dm} = 2×10^{15} $M_\odot$, M_{gas} = 10^{14} $M_\odot$, and a total stellar mass $M_\star$ = 2×10^{13} $M_\odot$.

Select epochs from the simulation are shown in Fig. 3. A head on collision between two subclusters, each with a mass of $\sim 8\times10^{14}$ $M_\odot$ begins at $z \sim 0.5$. The first core passage occurs at $z \sim 0.35$ and the cores merge at $z \sim 0.2$. An animation of the X-ray surface brightness and the projected, emission-weighted temperature map is available from the conference website. The movie follows the formation of the cluster from a redshift of 4 to the present epoch and shows a comoving region

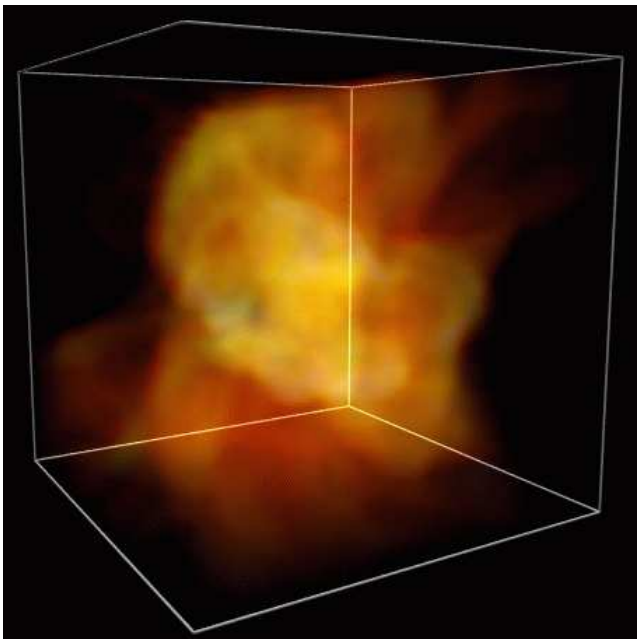

Figure 4: The three dimensional temperature field from our example cluster at an epoch of z = 0.26. The bounding box is $8h^{-1}$ Mpc on a side comoving and the color coding varies from white for the hottest gas through yellow, orange and red for the cooler gas.

$8h^{-1}$ Mpc on a side.

A rendered animation of the three-dimensional temperature field is also available. One time slice (at $z \sim 0.25$) from this animation is shown in Fig. 4. The hottest gas is white and we can identify several hot shock fronts expanding out from the cluster as a consequence of the major merger event. Note how aspherical and irregular the temperature structure is.

The animations also illustrate the dynamical nature of clusters. To quantify the importance of cluster interactions, we have performed a β model analysis of the thermal SZE and X-ray images taken at $\sim$ 350 time slices from the simulation. We construct projected images of the Compton parameter

$$y = \int \sigma_T n_e \frac{k_b T}{m_e c^2} dl \tag{4}$$

and, effectively, the X-ray emission measure (we do not include cosmological dimming and focus instead on the intrinsic emission from the cluster)

$$S_X = \int n_e n_H \Lambda(T)\, dl \tag{5}$$

Here l is the independent variable along the line of sight, σ_T is the Thompson cross section, n_e is the electron number density, n_H is the proton number density, k_b is Boltzmann's constant, T is the temperature, $m_e c^2$ is the electron rest mass energy and the function $\Lambda(T)$ is the emissivity for a 0.3 solar metallicity plasma.

We identify halos within the data sets and construct azimuthally-averaged profiles about the center of mass of the cluster. At high redshifts, before the cluster forms, we track the initially most massive sub-cluster from one time slice to the next. If we assume that the gas density follows an isothermal β model, y and S_X at projected radius b are given by

$$y(b) = y_0 \left(1 + \left(\frac{b}{r_c}\right)^2\right)^{\frac{1}{2} - \frac{3}{2}\beta} \tag{6}$$

$$S_X(b) = S_{X0} \left(1 + \left(\frac{b}{r_c}\right)^2\right)^{\frac{1}{2} - 3\beta} \tag{7}$$

We jointly fit both equations to obtain the best fit parameters y_0, S_{X0}, r_c, and β. The resulting time sequence of model parameters are shown in Fig. 5 where S_X has been normalized by its maximal value. The major merger is clearly evident as a strong boost of the thermal SZE and X-ray data at 10 Gyr. Beyond that point to the present epoch, the cluster does not interact with any system more massive than about 10% of the cluster's mass, indicating that the significant variations are due to minor mergers. Looking into the past, we note a major merger at $z \sim 1$ and strong variations as multiple clumps collide and merge at higher redshifts.

During the major merger at 10 Gyr, the thermal SZE is boosted by a factor of $\sim$ 10 with the rise and fall back to equilibrium values occurring over $\sim$ 1 Gyr. In terms of the X-ray, the central emission measure is boosted by $\sim$ 20 at its maximum and then S_{X0} falls by a factor of $\sim$ 50 until equilibrium values are again attained. By way of comparison, if we assume an isothermal β model (and that β is independent of mass while the cluster core radius, r_c, is proportional to the virial radius), simply doubling the cluster mass boosts S_{X0} by $2^{2/3}$ and y_0 doubles. Merger events significantly complicate the mapping between cluster observables and the fundamental cluster parameter, its mass.

3 An additional argument for AGN feedback

Entropy is a convenient measure of the thermal state and history of gas in clusters (Voit & Bryan, 2001). We use the quantity $S = T n_e^{-2/3}$ to trace the gas entropy. In a recent compilation, Ponman et al. (2003) have assembled measurements of S at one tenth of r_{200}

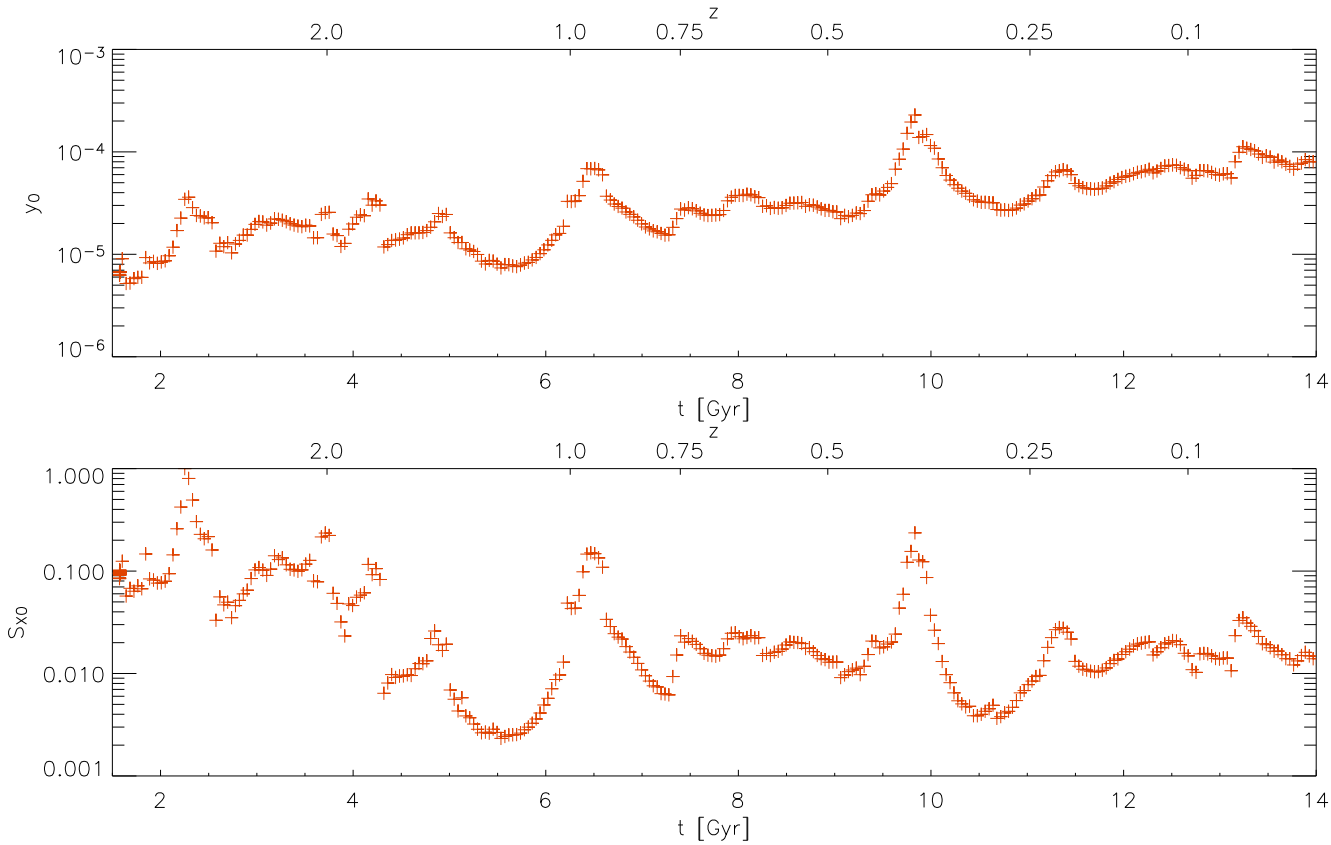

Figure 5: The "light curves" for one particular clump that becomes part of the most massive cluster in our sample. The panels show the β model parameters for the central Compton parameter (y_0) and X-ray surface brightness (S_{X0}) from a simultaneous fit.

for 66 clusters and groups (including two isolated, giant ellipticals). With self-similar scaling, one expects $S \propto T$. Instead, Ponman reports that S = 124 $T^{0.65}$ keV cm^2 and this deviation is claimed as evidence for non-gravitational heating in clusters and groups, presumably arising from galaxy formation.

To investigate this result, we have compiled samples of $\sim$ 400 halos at the present epoch evolved in the adiabatic limit and with the addition of cooling, star formation and supernova feedback. We plot these simulated halos in the $S\left(r = 0.1r_{200}\right) - T_{\rm virial}$ plane in Fig. 6. The least-squares scaling relation from the 100 most massive halos in the adiabatic sample has a slope of 1, consistent with self-similar scaling, while the star formation with feedback sample has a slightly steeper slope of 1.1. The Ponman relation is also plotted in Fig. 6 as a dotted line. Although there is significant scatter, most of the simulated clusters lie below the observed relation in the regime of poor clusters and groups (systems with $T_{\rm virial} \sim$ 1–2 keV). As the simulations with star formation and supernova feedback incorporate the positive feedback of galaxy formation, this discrepancy may indicate that additional heating from AGN is required to bring the simulations into agreement with observed clusters.

4 Constraints from testbed clusters

As has been argued in the previous discussion, detailed energy balance in the baryonic component of clusters entails, in general, the interaction of multiple coupled and competing process. In the face of this complexity, observations of individual clusters where specific processes can be isolated and studied independently will be most useful. In particular we are interested in clusters that (1) appear to be dynamically relaxed with no evidence for recent mergers that could drive the clusters out of equilibrium (2) lack evidence for AGN outbursts in their X-ray and radio emission and (3) posses canonical cool cores where the temperature falls by a factor of $\sim$ 3 in the cluster center.

We have analyzed a 45 ks *Chandra* ACIS-I observa-

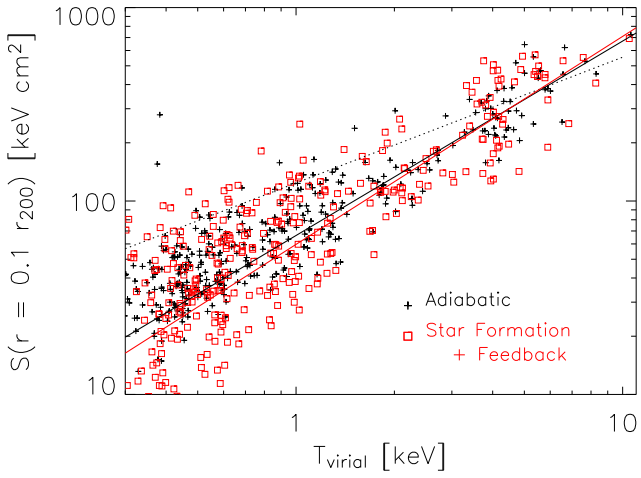

Figure 6: The entropy of the cluster gas at a fiducial radius of 0.1 r_{200} plotted against the halo's virial temperature for $\sim$ 400 halos evolved in the adiabatic limit (black crosses) and with star formation and supernovae feedback (red squares). The solid black and red lines indicate the best fit relations for the 100 most massive halos in the adiabatic and star formation with feedback samples respectively. For both samples, the slopes are $\sim$ 1. The dotted line corresponds to the scaling relation derived by Ponman et al. (2003).

tion of the poor cluster of galaxies AWM7 which we identify as a possible testbed cluster that satisfies these three conditions. The top panel of Fig. 7 shows the adaptively smoothed X-ray image from the central $\sim$ 150 kpc region of the cluster. The cluster appears relaxed and elongated with no evidence for sharp edges in the surface brightness arising from shock fronts or cold fronts. The bottom panel of Fig. 7 shows the temperature map derived from spectral fits to adaptively binned regions in the cluster. Beyond the cooler core region, the temperature is remarkably uniform throughout the cluster. The projected temperature profile for AWM7 is plotted in Fig. 8. The temperature declines by a factor of $\sim$ 3 as has been reported for a number of cool core clusters.

The galaxies within the core region all appear to be radio quiet (Burns, 1990), including the cD galaxy, and there is no evidence for X-ray bubbles or cavities indicating that the cluster is not currently being heated by a feedback cycle nor has the cluster experienced an outburst in the recent past (up to the bubble rise and disruption time of $\sim 10^8$ yr). Therefore the gas in the core is either cooling currently or it is being maintained in a steady state by thermal conduction. Using the methodology of Medvedev et al. (2003), we find that AWM7 is

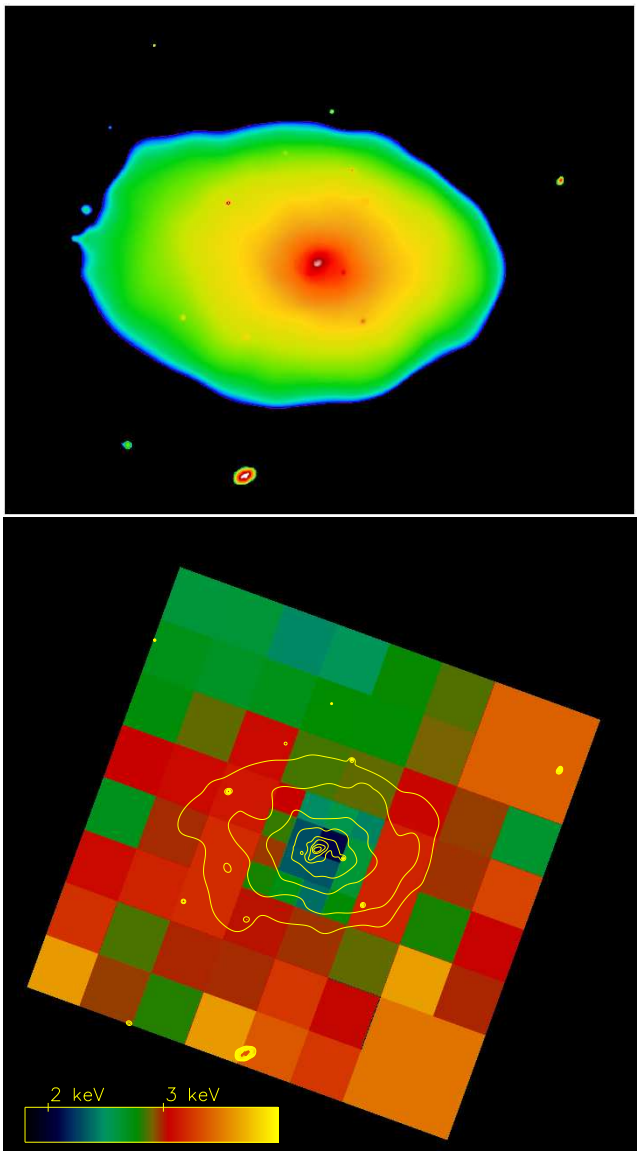

Figure 7: Adaptively smoothed *Chandra* image of the core region of AWM7 in the 0.7–10 keV band (top image), and the corresponding temperature map (bottom image) with X-ray contours overlaid.

consistent with thermal conduction balancing radiative cooling for a suppression factor, $f \sim 0.2$.

5 Conclusions

- Energy balance in clusters requires the interplay of several coupled mechanisms
- Thermal conduction from the hot envelope into cluster cores can be comparable in magnitude to radiative losses alone
- AGN feedback is likely to also play an important

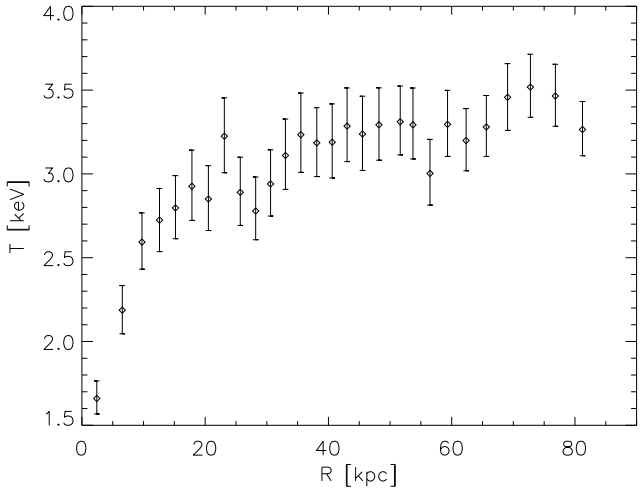

Figure 8: The projected temperature profile for AWM7 derived from spectral fits to the azimuthally-averaged cluster emission. AWM7 displays a canonical cool core but there is no evidence for a cooling flow.

role in cluster cores

- Clusters are inherently dynamic, geometrically complex systems
- Major mergers can significantly boost observational signatures from their equilibrium values (e.g., factor of ~ 10 boost in the the central thermal SZE and ~ 20 in the central X-ray surface brightness) for periods comparable to the dynamical time.
- Need to observe clusters without X-ray bubbles where astrophysical mechanisms controlling energy balance can be isolated

Acknowledgments

We thank Michael Norman, Greg Bryan and the Laboratory for Computational Astrophysics for development and support of the ENZO code. We also wish to acknowledge the NCSA for a grant of time on supercomputing platforms and support from NASA through the *Chandra* X-ray Observatory Center grant TM3-4008A.

References

Blanton, E. L., Sarazin, C. L., McNamara, B. R., Wise, M. W. 2001, ApJ, 558, L15

Burns, J. O. 1990, AJ, 99, 14

Cen, R., Ostriker, J. P. 1992, ApJ, 399, 113

Cho, J., Lazarian, A., Honein, A., Knaepen, B., Kassinos, S., Moin, P. 2003, ApJ, 598, 77

Fabian, A. C., Sanders, J. S., Ettori, S., Taylor, G. B., Allen, S. W., Crawford, C. S., Iwasawa, K., Johnstone, R. M., Ogle, P. M. 2000, MNRAS, 318, L65

Heinz, S., Choi, Y.-Y., Reynolds, C. S., Begelman, M. C. 2002, ApJ, 569, L79

Johnstone, R. M., Allen, S. W., Fabian, A. C., Sanders, J. S. 2002, MNRAS, 336, 299

Loeb, A. 2002, NewA, 7, 729

McNamara, B. R., Wise, M., Nulsen, P. E. J., David, L. P., Sarazin, C. L., Bautz, M., Markevitch, M., Vikhlinin, A., Forman, W. R., Jones, C., Harris, D. E. 2000, ApJ, 534, L135

McNamara, B. R., Wise, M. W., Nulsen, P. E. J., David, L. P., Carilli, C. L., Sarazin, C. L., O'Dea, C. P., Houch, J., Donahue, M., Baum, S., Voit, M., O'Connell, R. W., Koekemoer, A. 2001, ApJ, 562, L149

Medvedev, M. V., Melott, A. L., Miller, C., Horner, D. astro-ph/0303310

Motl, P. M., Burns, J. O., Loken, C., Norman, M. L., Bryan, G. L. 2004, ApJ,

Narayan, R., Medvedev, M. 2001, ApJ, 562, 129

Omma, H., Binney, J., Bryan, G., Slyz, A. 2004, MNRAS, 348, 1005

Ponman, T. J., Sanderson, A. J. R., Finoguenov, A. 2003, MNRAS, 343, 332

Ruszkowski, M., Begelman, M. C. 2002, ApJ, 581, 223

Voit, G. M., Bryan, G. L. 2001, Nature, 414, 425